# Dislocation Intersections and Reactions in FCC and BCC Crystals

Ladislas P. Kubin, Ronan Madec[1] and Benoit Devincre
Laboratoire d'Etude des microstructures, CNRS-ONERA,
29 Av. de la Division Leclerc, BP 72, 92322 Chatillon Cedex, France
[1]Now at: DPTA, Commissariat à l'Energie Atomique, BP12, 91680 Bruyères-le-Châtel, France

## ABSTRACT

The various types of configurations formed in face-centered cubic (fcc) and body-centered cubic (bcc) structures by two interacting, non-coplanar, dislocation segments of various orientations are examined and discussed. The focus is on junction formation and on a particular interaction, the collinear interaction, which deserves much more attention than paid up to now.

## INTRODUCTION

As first stated by Taylor [1], strain hardening in crystals stems from dislocation interactions. Within the widely accepted "forest model" [2, 3], the formation and the destruction of junctions or locks produced by attractive interactions between non-coplanar dislocations contribute to most of the flow stress in conditions of multiple slip. The stability of junctions is governed by self-energies, which are mainly elastic in nature since the contribution of the dislocation cores is comparatively negligible. This allowed performing studies on particular junction configurations in several simple crystal structures, fcc [4, 5], see also [6], bcc [7, 8] and hexagonal close-packed [9]. More recent studies of individual junction configurations at the atomic scale [10, 11] and at the mesoscopic scale [12-15] have confirmed the validity of such elastic approaches. At the mesoscale, however, analytical elastic calculations cannot fully account for the mutual distortions of interacting dislocations lines. This is why dislocation dynamics (DD) simulations are particularly suited for a more precise treatment of such problems.

The aim of the present study is to provide a global insight into the interactions and reactions of two dislocation segments in fcc and bcc crystals, stressing their dependence on the initial orientation of the lines. Some aspects of the simulation technique used in the present study are summarized. Mappings of dislocation reactions are then presented and discussed, with emphasis on an intersection process which has been largely ignored up to now and has recently be found to be of prominent importance, the collinear interaction. Concluding remarks are finally presented.

## METHODOLOGY

Use is made of a DD simulation, in which segments with a finite set of orientations are embedded into an elastic medium and move by discrete translations in an underlying mesoscopic lattice with same symmetry elements as the considered crystal. An early version of this simulation, in which continuous dislocation shapes were discretized into edge and screw segments, has been described is some detail [16, 17]. The updated version used in the present work is based on the same principles, which are discussed in [15, 18], but makes use of an

improved description of the dislocation lines. This allows one to treat dislocation reactions in a very precise, parameter-free, manner by incorporating the directions of dislocation reactions in the elementary base of vectors of the simulation [19, 20]. We focus here on the procedure for producing the intersection mappings shown in the next parts.

## Optimized Discretization of the Dislocation Lines

Figure 1 illustrates, through the example of Frank-Read sources in fcc and bcc crystals, how the discretization of the dislocation lines in the DD simulation can be adapted to different crystallographic structures. An extension to the treatment of prismatic and first-order pyramidal slip in hcp crystals will be described in a separate publication (Monnet et al., to be published).

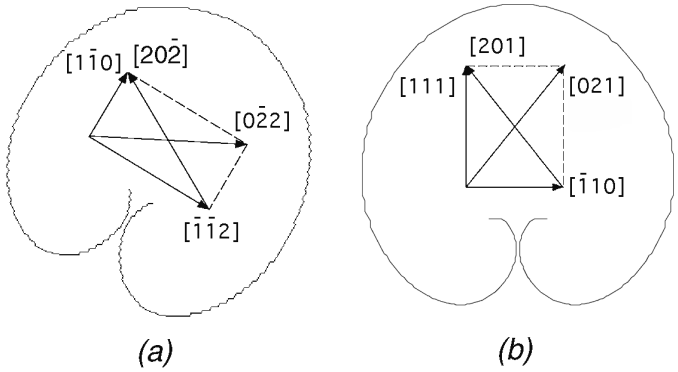


**Figure 1.** Frank-Read sources expanding under stress in their slip planes in the absence of lattice friction. The source segments are of edge character and of length 4 μm. The detail of the loops shapes is mostly determined by the loading conditions. (*a*) - $1/2[1\,\bar{1}\,0](111)$ slip in a fcc crystal (Cu). (*b*) – $1/2[111](11\bar{2})$ slip in bcc Ta. The <021> directions are those obtained by reaction of the slip systems $[111](11\bar{2})$ and $[1\,\bar{1}\,\bar{1}]\,(1\,\bar{1}\,2)$.

In the fcc structure (Fig. 1-a), the glide loops are described using a base of 8 line directions per slip plane, namely the edge, screw, $\pi/3$ and $2\pi/3$ directions with their two signs. In the bcc structure, 6 line directions per slip plane (two screw and four mixed) are sufficient if only {110} slip is accounted for. In order to treat all the junction formed by dislocations gliding in {110} and {112} planes, 12 and 20 lines directions are needed in {110} and {112} planes, respectively. The <021> directions shown in Fig. 1-b are those obtained by reaction of the slip systems $1/2[111](11\bar{2})$ and $1/2[1\,\bar{1}\,\bar{1}]\,(1\,\bar{1}\,2)$.

## Mappings of Dislocation Reactions

We consider the two slip systems (1) and (2) defined by their Burgers vectors $\boldsymbol{b}_i$ ( $i = 1, 2$) and their slip plane normal $\boldsymbol{n}_i$. Along the intersection of the two slip planes, where junctions potentially form, a reference direction is chosen, $\boldsymbol{l}_j$. The interacting segments, each in one slip

plane, have line direction $\boldsymbol{l}_i$ (i = 1, 2). They are initially of same length and intersect each other in their midpoints (Fig. 2), making angles $\phi_1$ and $\phi_2$, respectively, with respect to $\boldsymbol{l}_j$. These angles are measured in reference frames such that $\boldsymbol{n}_1 = -\boldsymbol{b}_1 \times \boldsymbol{l}_1$ and $\boldsymbol{n}_2 = \boldsymbol{b}_2 \times \boldsymbol{l}_2$. With this convention, two dislocation lines parallel to $\boldsymbol{l}j$, ($\phi_1 = \phi_2 = 0$) and with opposite Burgers vector are attractive.

After relaxation, three types of configurations are obtained, which are illustrated in Fig. 2. Figs. 2-a and 2-c show two configurations corresponding to junction formation and repulsive interaction, respectively. A third type of configuration occurs, in which although two segments are attractive, the formation of a junction is not observed because it is not energetically favored. An example of such configuration is shown in Fig. 2-b; it is called a crossed-state after Wickham et al. [12]. The occurrence of crossed-states can be understood from a simple geometrical argument given by Friedel [3]. When a junction is formed, equilibrium at the triple nodes corresponds to a certain angle between the arms of the initial segments. This angle is necessarily larger than its value before junction zipping (cf. Fig. 2-a). Thus, if the two interacting segments initially make an angle larger than the equilibrium value, and even if they are attractive, no line tension equilibrium can be achieved and no junction can be formed. A last type of configuration consists of a few neutral states that cannot be characterized due to the too small magnitude of the interactions. For the sake of simplicity, neutral states and crossed-states are lumped into a common category of weak obstacles.

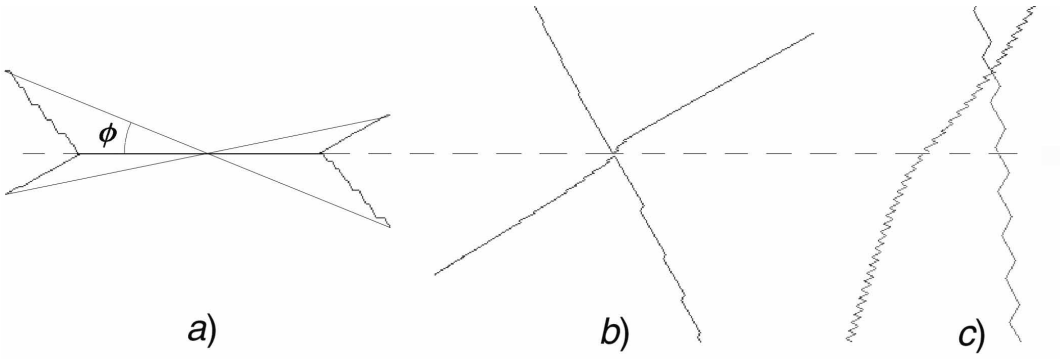


**Figure 2**. Three simulated configurations of intersecting non-coplanar segments gliding in different slip planes. The dashed line represents the direction of intersection of the two slip planes. (*a*) - Attractive interaction: junction formation. The thick lines represent the initial configuration. (*b*) - Crossed-state: although the two segments are attractive, junction formation is not energetically favored. (*c*) - Repulsive interaction: the two segments move away from each other.

The simulation of dislocations interactions and reactions is performed as follows. For a given set of interacting slip systems and for a couple of initial orientations of the dislocation lines, an initial configuration is built up. We consider two straight segments pinned at their extremities in order to mimic strong interactions occurring in real crystals with other forest dislocations. For the same reason, the initial length of the segments is taken to be $l_i \approx \rho_f^{-1/2} = 1$ μm, the typical length associated with a forest density $\rho_f = 10^{12}$ m$^{-2}$. To discuss the influence of the segment's length, another length of 30 μm is also used in Fig. 7, below. This second type of configuration is dedicated to a comparison with simplified analytical models, which consider

infinite dislocation lines. In the initial state, the midpoints of the two segments are placed at an approach distance of $d \approx l_i/100$. Then, the two segments are let to relax and reach an equilibrium configuration such that the Peach-Koehler force on each discretized segment describing the lines is equal to zero. To speed up relaxation, the stress vs. velocity law is in all cases the one defined for fcc crystals, which entails high dislocation mobility. Isotropic elasticity is used throughout the present work. The simulated model materials are defined by their Burgers vector, Poisson's ratio, $\nu$, and isotropic shear modulus, $\mu$. The values used are $b$ = 0.256 nm, $\nu$ = 0.347 and $\mu$ = 42 GPa for fcc crystals and $b$ = 0.286 nm, $\nu$ = 0.33 and $\mu$ = 68.5 GPa for bcc crystals. However, within the restriction of isotropic elasticity, all the mappings presented in the next sections are generic and apply to all materials of same crystallographic structure. The reason is that within the present context, the configurations investigated depend on elastic interaction and line tension forces that scale with the product $\mu b$. Changes in the Poisson's coefficient from one material to the other induce only minor modifications.

The boundary conditions of the simulations are chosen in order to investigate the properties of two isolated dislocations embedded into an infinite elastic medium. This configuration can easily be obtained with the help of periodic boundary conditions in a reference cell at least two times larger than the initial length of the dislocation lines. The nature of the relaxed configuration is identified as follows. If the two dislocation lines superimpose each other over a fraction of their length, the formation of a junction is stated. If the shortest approach distance between the dislocations has increased after relaxation, the configuration is necessarily repulsive. All the intermediate cases not accounted for by the above two criteria, are considered as cross-states.

The output of the simulations is presented for each couple of angles ($\phi_1$, $\phi_2$) in the form of a mapping indicating the nature of the final state, like in previous works on bcc metals [7, 12]. The properties of junctions, like their length or critical unzipping stress, can be derived easily from these results [15, 18], but will not be reported here in detail by lack of space.

## Comparison With Elastic Calculations

Two elastic solutions, which derive from simplified models, yield boundaries that are superimposed to the computed mappings presented below. They are aimed at providing a guide and a check from elastic solutions less sophisticated than those given by the simulations. A first boundary is the locus of the points where junction formation is neutral, i.e., neither favored nor forbidden. This criterion can be obtained either by a condition of line energy minimization or equivalently by the condition of line tension equilibrium at the triple nodes. It is calculated for straight segments, in isotropic elasticity and with an orientation-dependent line tension that does not include the usual logarithmic term. The corresponding expression can be derived easily [21]. The second boundary delimitates the border between initially attractive and repulsive segments. It is calculated from the interaction force along the shortest approach distance of two rigid, infinite, lines. Kroupa [22] gave a simple solution to this problem (see also [23]). Both models assume that the interacting segments are rigid but, as discussed below (cf. Fig. 4), they may also lead to opposite predictions regarding the nature of the final state. The comparison with the simulations is nevertheless useful for the interpretation of the results.

## JUNCTIONS IN FCC AND BCC CRYSTALS

### Junctions in FCC Crystals

Figure 3 shows the mappings obtained for the three types of slip systems interactions leading to perfect junctions in the fcc structure: - the Lomer junction, of 1/2<110> type, which is sessile, - the glissile junction, also of 1/2<110> type, which is glissile in one of the two intersecting slip planes, and - the Hirth lock, where the interacting Burgers vectors are orthogonal and the reaction product is of the <200> type. The solutions of the two simple elastic models mentioned above are superimposed to the simulation results.

The three configurations depicted in Fig. 2 are found in these graphs. The mappings are periodic with a period ($\phi_1 = \pm \pi$ , $\phi_2 = \pm \pi$), since these translations leave the initial configuration

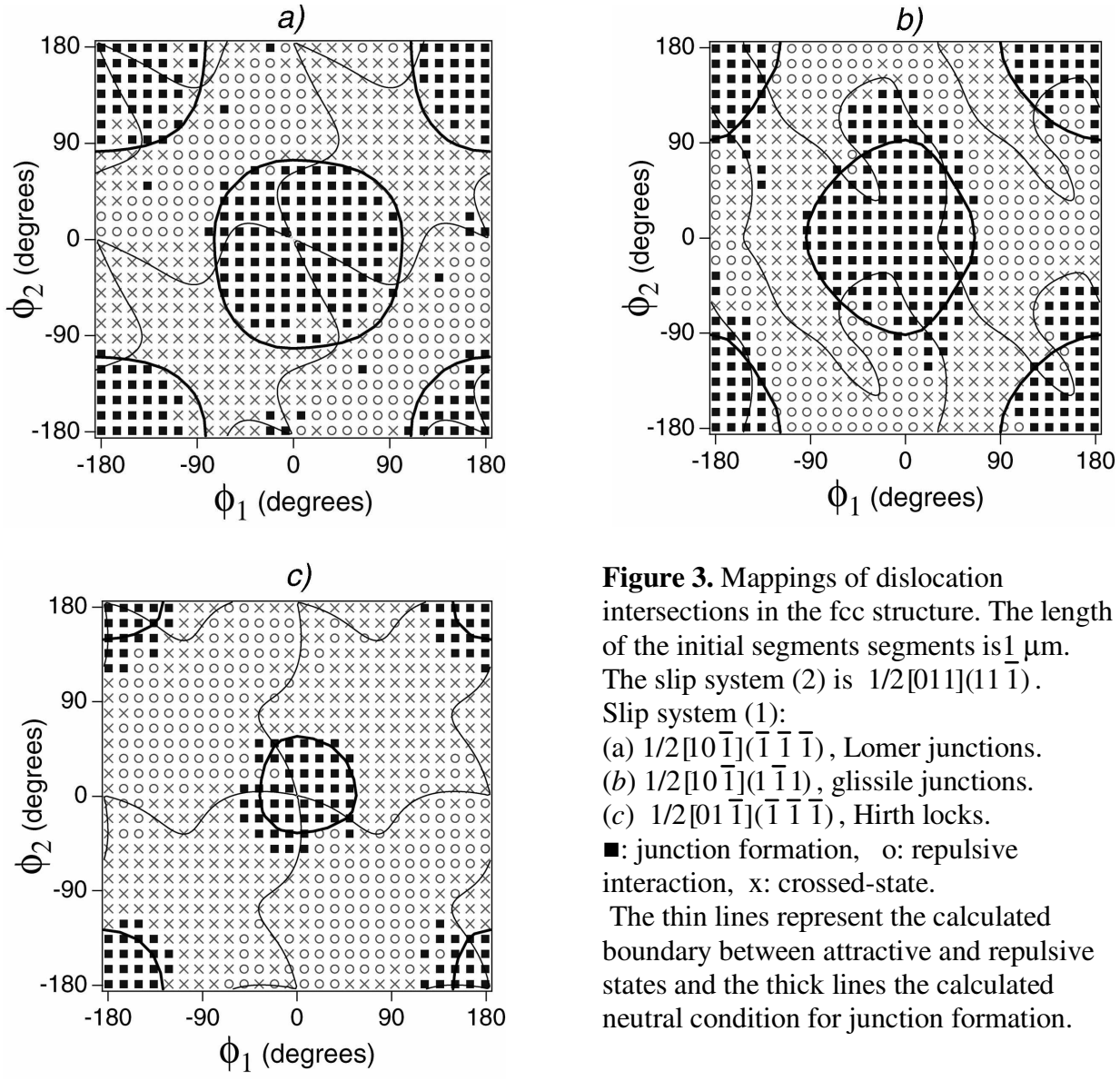


**Figure 3.** Mappings of dislocation intersections in the fcc structure. The length of the initial segments segments is 1 μm. The slip system (2) is $1/2[011](11\bar{1})$. Slip system (1):
(a) $1/2[10\bar{1}](\bar{1}\,\bar{1}\,\bar{1})$, Lomer junctions.
(*b*) $1/2[10\bar{1}](1\,\bar{1}\,1)$, glissile junctions.
(*c*) $1/2[01\bar{1}](\bar{1}\,\bar{1}\,\bar{1})$, Hirth locks.
■: junction formation, o: repulsive interaction, x: crossed-state.
The thin lines represent the calculated boundary between attractive and repulsive states and the thick lines the calculated neutral condition for junction formation.

unchanged (cf. Fig. 2-a). The domain of junction formation takes the form of lobes encircling the origin. These lobes depart from a circular shape due to the orientation-dependence of the line tension and approximately follow the predictions of the elastic models (thick lines in Fig. 3). The boundary between attractive states, i.e., junctions and crossed-states, and repulsive states is also relatively well accounted for by Kroupa's formula (thin lines in Fig. 3). The assumptions made in the two elastic estimates also manifest themselves for some orientations through conflicting predictions, as is clearly seen in the case of the glissile junction. In Fig. 3-b, on top of the central lobe, junctions are formed between attractive segments, whereas for rigid segments the reaction is energetically unfavorable. Inversely, at the bottom of the upper lobe at right, junction formation is energetically favorable for rigid segments, but does not occur because the segments are repulsive. Such discrepancies stem from the fact that the two elastic estimates reflect in an imperfect manner two aspects of the same global behavior. The junction lobes derive from a simplified calculation of the energies of the initial and final states, whereas the boundary between attractive and repulsive states derives from a calculation of the initial interaction force, i.e., of the initial derivative of energy vs. reaction coordinate. As illustrated by 4, the two estimates may yield opposite predictions in the presence of an energy barrier. Whether or not the latter can be overcome by the dislocations depends on some complex balance between line tension and interaction forces, as will be discussed in the next part.

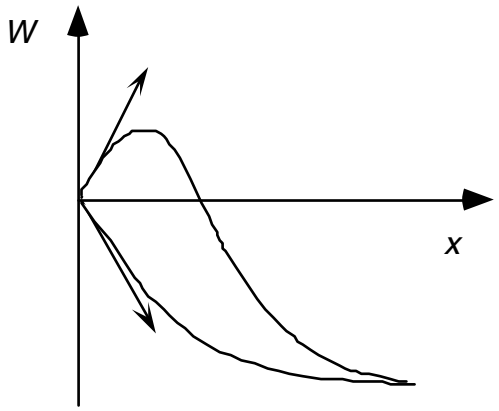


**Figure 4.** Schematic diagram of elastic energy ($W$) vs. reaction coordinate ($x$) for junction formation. A calculation of elastic energy predicts junction formation if the final state has a lower energy than the initial state. The initial slope yields the initial interaction force. If it is positive, the initially repulsive dislocation can reach the state of minimum energy only if they are able to overcome an energy barrier.

According to the forest model [2, 4], the strength of junctions is, in first approximation, inversely proportional to the length of the initial segments. It also exhibits a geometrical dependence on the angles ($\phi_1$, $\phi_2$), which is slightly anisotropic due to the orientation dependence of the line tension. One may note that the strength of a junction is by definition zero at the transition between junctions and other states, so that the periphery of the junction lobes corresponds to the weakest configurations. This strength diverges at the origin, since the two parallel lines are fully recombined. Indeed, the length of residual arms being zero, an infinite stress is required to unzip the junction. Assuming than the global strength of an interaction is mostly due to junctions and depends on the area enclosed by the junction lobes, we see that the glissile and Lomer junctions should have rather comparable strengths, whereas the Hirth lock, whose stability is due to the orientation-dependence of the line tension, is a rather weak obstacle. Many other details can be inferred from simple considerations. For instance the lobe of the glissile junction is elongated along the y-axis because the segment (2) is of edge character at $\phi_2 = \pi/2$. It has a high elastic energy, which favors junction formation.

**Junctions in BCC Crystals**

In bcc crystals, dislocations of Burgers vector 1/2<111> principally glide in {110} and {112} planes. Püschl [7], has classified the different types of interactions in the course of a detailed study of the stability of junctions in anisotropic elasticity. The reaction product is always found to be of the <100> type. For dislocations reacting in {110} planes and forming stable junctions, three different types of mapping configurations are obtained. By reason of symmetry it is sufficient to consider the interaction of a primary system, for example $1/2[111](\bar{1}10)$, with any other Burgers vector and the three slip planes that contain it, for example $1/2[1\bar{1}1](011)$, $1/2[1\bar{1}1](\bar{1}01)$ and $1/2[1\bar{1}1](110)$. One can easily check that in the first case, the [010] junction is sessile and of mixed character ($\boldsymbol{l}_j = [11\bar{1}]$). In the second case, it is also of mixed character ($\boldsymbol{l}_j = [111]$), but glissile in $(\bar{1}01)$. Wickham et al. [12] have studied the two related mappings. The third case is illustrated by Fig. 5-a; it corresponds to a sessile edge junction of line direction $\boldsymbol{l}_j = [001]$. Due to the multiplicity of additional reactions arising when {112} slip systems are accounted for, only one example is shown here (Fig. 5-b).

The qualitative considerations developed in the previous section also apply to the present case. From the viewpoint of junction stability, the main difference between fcc and bcc crystals resides in the higher energy of the reaction product in bcc crystals, since its Burgers vector squared is larger than that of the parent segments by a factor of 4/3. This results in smaller junction lobes, as compared to those of the glissile or Lomer junctions (cf. Figs. 3-a and 3-b).

At low temperature and in the presence of a lattice friction on screw dislocations, dislocation loops become elongated in the screw direction, which is that of the less mobile species. As plastic flow is mostly governed by the properties of screw dislocations, strain hardening

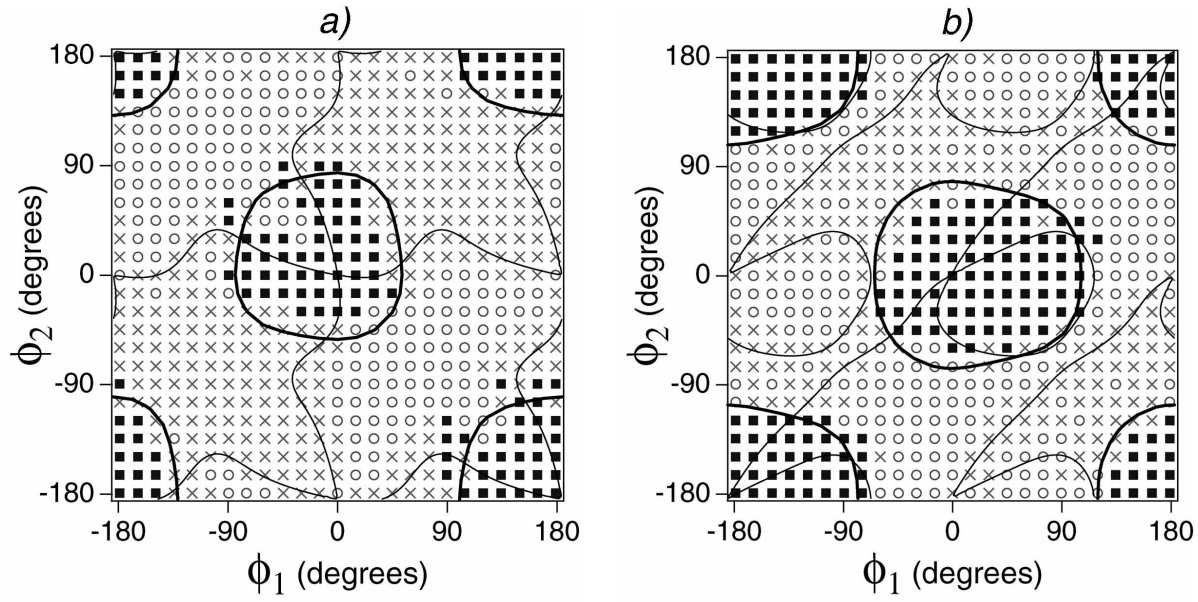


**Figure 5**. Mappings of dislocation intersections in the bcc structure. The symbols have same meaning as in Fig. 3. The length of the interacting segments is 1 μm. Slip system (1): $1/2[111](\bar{1}10)$. System (2) : (*a*) $1/2[1\bar{1}1](\bar{1}\,\bar{1}0)$, (*b*) $1/2[1\bar{1}\,\bar{1}](\bar{1}1\bar{2})$.

essentially depends on the interactions between screw dislocations and the forest. Then, the mappings reduce to a set of horizontal and vertical data lines drawn for segments with screw orientation, from which one can deduce the characters of the forest dislocation lines that strongly interact with screw dislocations.

Finally, in bcc metals and at low temperature, the flow stress is a complex superposition of friction stress and forest density, and it is not proportional to the square root of the forest density as in fcc crystals [24]. A screw dislocation line pinned between two obstacles does not achieve equilibrium bowed-out shapes under increasing stress. Rather, the screw portions move forwards by the thermally assisted nucleation of kink-pairs. Thus, all the dislocation movements associated with junction formation and unzipping are sensitive to the applied strain rate or temperature and kinetic effects can no longer be ignored. In short, the mappings presented here are only meaningful in the absence of lattice friction, i.e., at high temperatures.

## THE COLLINEAR INTERACTION

To each slip system is associated a cross-slip system with same (collinear) Burgers vector; the two slip planes intersect along a line parallel to their common Burgers vector. The non-screw dislocations of each system play the role of forest obstacles with respect to the dislocations of the other system and their interaction is called the collinear interaction. Upon intersection, mutual annihilation of the lines can take place according to the reaction $\boldsymbol{b}_1 - \boldsymbol{b}_1 = 0$, which is equivalent to the formation of a highly stable junction with zero Burgers vector. A simulated sequence of collinear annihilation is shown in Fig. 6.

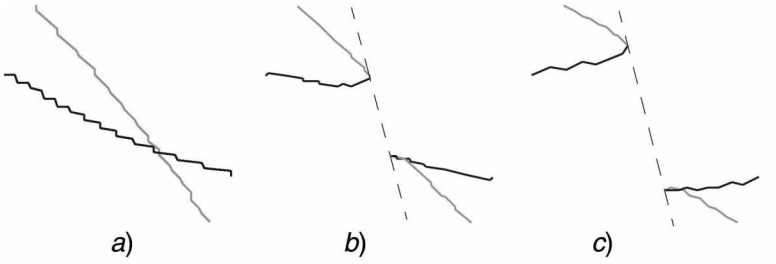


**Figure 6**. Simulation of collinear annihilation in the fcc structure. (*a*) – The initial configuration consists of two non-coplanar, attractive lines, of mixed character and with Burgers vectors of opposite sign. (*b*) – Annihilation takes place along the direction of intersection of the two slip planes (dashed line), which is parallel to $\boldsymbol{b}$. (*c*) - The final configuration is made up of two composite segments in equilibrium at double nodes along the intersection of the two slip planes.

For the collinear interaction in fcc crystals, there is only one type of mapping per Burgers vector. Figs. 7-a and 7-b, were obtained for segments of respective lengths 30 and 1 microns, respectively, in order to illustrate a length effect that is discussed below. If one considers the interactions of {110} and {112} slip systems in bcc crystals, there are three different

configurations for the collinear interaction: one only for the interaction between crystallographically equivalent slip systems and two between {110} and {112} slip planes, of which one is shown in Fig. 7-c.

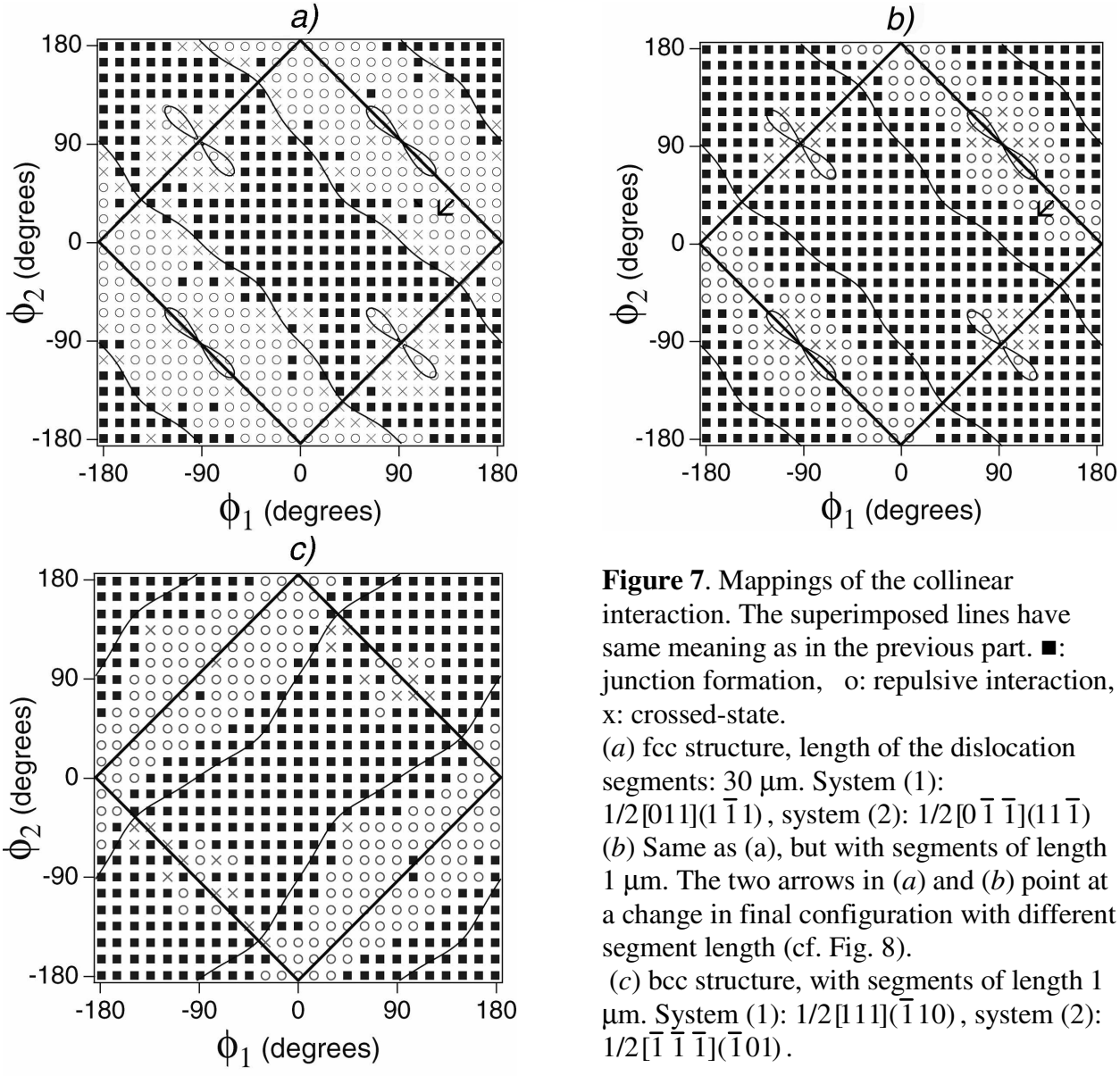


**Figure 7**. Mappings of the collinear interaction. The superimposed lines have same meaning as in the previous part. ■: junction formation, o: repulsive interaction, x: crossed-state.
(*a*) fcc structure, length of the dislocation segments: 30 μm. System (1): $1/2[011](1\bar{1}1)$, system (2): $1/2[0\bar{1}\bar{1}](11\bar{1})$
(*b*) Same as (a), but with segments of length 1 μm. The two arrows in (*a*) and (*b*) point at a change in final configuration with different segment length (cf. Fig. 8).
(*c*) bcc structure, with segments of length 1 μm. System (1): $1/2[111](\bar{1}10)$, system (2): $1/2[\bar{1}\,\bar{1}\,\bar{1}](\bar{1}01)$.

As in the previous part, predictions from the elastic theory of dislocations are superimposed to the simulation results. In contrast to the case of junctions, the total elastic energy is always reduced by the collinear annihilation, except along the singular lines $\phi_1 \pm \phi_2 = \pm\pi$. Along these lines, the two initial segments have same character and their projected line tensions exactly balance in projection along $\boldsymbol{l}_i$. Thus, the initial configuration is already in equilibrium. According to Kroupa's formula, the repulsive and attractive states are localized in parallel bands of same total area since half of the configurations are repulsive (or attractive). There are, in Figs.

7-a and 7-b, four small double lobes centered on the orientation $\phi_1 = \phi_2 = \pm \pi/2$, inside which the interaction changes sign. This orientation corresponds to non-interacting initial segments perpendicular to $\boldsymbol{l}_i$ and of edge character. The bcc mapping (Fig. 7-c) is rather similar, except that the boundary between attraction and repulsion no longer includes small localized domains where the interaction changes sign, but very flat local minima.

For long interacting segments (Fig. 7-a), the simplified elastic predictions are in very good agreement with the simulated results. The neutral states and crossed-states are localized near the singular lines and small lobes defined above. In contrast, with shorter segments length (Fig. 7-b, see also Fig. 7-c), the domain of collinear annihilation largely expands into the previous domain of neutral and repulsive states. The repulsive and neutral states are now localized around the regions of weak interaction and null energy balance. This predominance of collinear annihilations is due to the increased flexibility of the short dislocation lines, as induced by the logarithmic factor in the line tension [4, 15, 25]. This results in a reduction of the energy barrier opposing annihilation that is depicted in Fig. 4. Figure 8 illustrates this effect in the case of two initially repulsive straight lines. Thus, the average strength of the collinear interaction should be significantly larger than that of junctions, due to both the larger probability of occurrence of the reaction, as can be checked by comparing Figs. 3 and 7, and the higher stability of the final configuration. The interest of the collinear annihilation resides in the fact that it occurs in an athermal manner and induces annihilation events even in the absence of cross-slip. Other consequences of this interaction on dislocation microstructures and plastic flow will be discussed in a separate publication (Madec et al., submitted).

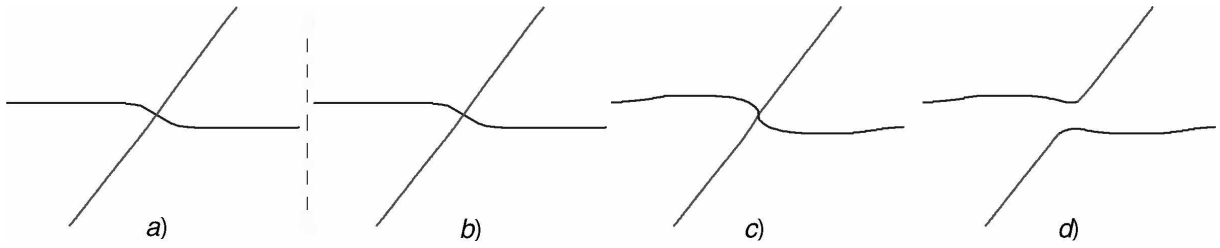


**Figure 8**. Interaction of two initially repulsive straight segments ($\phi_1 = 115°$ , $\phi_2 = 22°$, see arrows in Figs. 7-a and 7-b). The configurations are seen along the slip plane of the horizontal line. (*a*) - With segments of length 30 μm, a stable repulsive state is obtained. (*b*) to (*d*) - With segments of length 1 μm, the saddle point associated with the repulsive interaction can be overcome owing to a smaller line tension. The dislocation lines are then able to reach their minimum energy configuration corresponding to mutual annihilation.

## CONCLUDING REMARKS

The present study shows that DD simulations are well suited for predicting accurately the outcome of the interaction between two non-coplanar dislocation segments, in the absence of lattice friction. Checking the properties of these individual configurations is, in fact, a mandatory step, preliminary to any attempt at a quantitative investigation of forest hardening.

Although the present work was performed in isotropic elasticity, there are two manners to

perform a more refined treatment in anisotropic elasticity. An approximate procedure, which should capture most of the effects of anisotropy, consists in simply tabulating the anisotropic local line tension in DD simulations. Rigorous solutions can be obtained through the use of coupled DD and Finite Element codes. An illustration of the use of both methods can be found in [26].

The mappings presented here were obtained in the absence of applied stress. They are necessarily modified in the presence of an applied stress, from which one can infer for instance which types of junctions are unzipped the most easily. However, as the flow stress of a crystal depends on complex averages over individual configurations that are less simple than the symmetrical ones examined here, the question of forest hardening can be treated quantitatively only by performing mass simulations on large dislocation densities [15].

A detailed study of the collinear annihilation has been presented at the scale of individual configurations, showing that the annihilation of dislocations gliding in slip and cross-slip systems can occur easily and in an athermal manner. As this interaction leads to extremely stable reaction products, it has a significant impact on microstructures and flow properties (Madec et al., to be published). Its study also reveals a strong influence of the average length of the interacting lines through line tension effects. This effect also manifests itself on all the critical stresses for remobilizing dislocations segments blocked after a reaction. It is in no way negligible if one considers that the average dislocation density and segments length evolve by orders of magnitude along a stress-strain curve.

## ACKNOWLEDGEMENTS

The authors would like to thank Drs. Thierry Hoc and Ghiath Monnet for helpful discussions and contributions to the present work. RM gratefully acknowledges the support of the Centre Européen de Calcul Atomique et Moléculaire (CECAM).

## REFERENCES

1. G.I. Taylor, *Proc. Roy. Soc. A* **145**, 362 (1934).
2. G. Saada, *Acta Metall.* **8**. 841 (1960).
3. J. Friedel, 1967, *Dislocations* (Pergamon Press, 1964), p. 43.
4. G. Schoeck and R. Frydman, 1972, *Phys. Stat. Sol. (b)* **53**, 661 (1972).
5. W. Püschl, R. Frydman and G. Schoeck, *Phys. Stat. Sol. (a)* **74**, 211 (1982).
6. L. Dupuy and M. Fivel, *Acta Mat.* **50**, 4873 (2002).
7. W. Püschl, *Phys. Stat. Sol.* **90**, 181 (1985).
8. W. Püschl, *Phil. Mag. Lett.* **80**, 199 (2000).
9. W. Püschl and G. Schoeck, *Crystal Res. and Technology* **19**, 303 (1984).
10. V.V. Bulatov, F.F. Abraham, L.P. Kubin, B. Devincre and S. Yip, *Nature* **391**, 669 (1998).
11. D. Rodney and R. Phillips, *Phys. Rev. Lett.* **82**, 1704 (1999).
12. L.K. Wickham, K.Schwarz, and J.S. Stölken, Phys. Rev. Lett. **83**, 4574 (1999).
13. V.B. Shenoy, R.V. Kukta and R. Phillips, *Phys. Rev. Lett.* **84**, 1491 (2000).
14. C. Shin, M. Fivel, D. Rodney, R. Phillips, V.B. Shenoy and L. Dupuy, *J. Phys IV* (France) **11**, 19 (2001).
15. R. Madec, B. Devincre and L.P. Kubin, *Phys. Rev. Lett.* **89**, 255508 (2002).

16. L.P. Kubin, G. Canova, M. Condat, B. Devincre, V. Pontikis and Y. Bréchet, *Solid State Phenomena* **23**-**24**, 455 (1992).
17. B. Devincre and L.P. Kubin, 1997, *Mat. Sci. Eng. A* **234-236**, 8 (1997).
18. R. Madec, B. Devincre and L.P. Kubin, *Scripta Mater.* **47**, 689 (2002).
19. R. Madec, B. Devincre and L.P. Kubin, in *Multiscale Modeling of Materials – 2000*, ed. L.P. Kubin, R. Selinger, J.L. Bassani and K. Cho (Materials Research Society, 2000), Symposium Proceedings Vol. 653, p. z1-8.
20. R. Madec, *Ph.D. Dissertation*, University of Orsay (2001).
21. R. Madec, B. Devincre and L.P. Kubin, 2002c, *Comp. Mater. Sci*. **23**, 219 (2002).
22. F. Kroupa, 1961, *Czech. J. Phys. B* **11**, 847 (1961).
23. J. Hirth and J. Lothe, *Theory of Dislocations* (Krieger, 1982), p. 123.
24. M. Tang, B. Devincre, and L.P. Kubin, *Model. Simul. in Mat. Sci. Eng*. **7**, 893 (1999).
25. S.J. Basinski and Z.J. Basinski, in: *Dislocations in Solids*, ed. FRN Nabarro (North Holland, 1979), Vol. 4, p. 261.
26. S. Groh, B. Devincre, L. Kubin, A. Roos, F. Feyel and J.-L. Chaboche, *Phil. Mag. Lett*., **83**, 303, 2003.